ACS OMEGA

http://pubs.acs.org/journal/acsodf

Article

An *Ab Initio* Neural Network Potential Energy Surface for the Dimer of Formic Acid and Further Quantum Tunneling Dynamics

Fengyi Li, Xingyu Yang, Xiaoxi Liu, Jianwei Cao, and Wensheng Bian*

Cite This: *ACS Omega* 2023, 8, 17296−17303

Read Online

ACCESS | Metrics & More | Article Recommendations | Supporting Information

ABSTRACT: We construct a full-dimensional *ab initio* neural network potential energy surface (PES) for the isomerization system of the formic acid dimer (FAD). This is based upon *ab initio* calculations using the DLPNO-CCSD(T) approach with the aug-cc-pVTZ basis set, performed at over 14000 symmetry-unique geometries. An accurate fit to the obtained energies is generated using a general neural network fitting procedure combined with the fundamental invariant method, and the overall energy-weighted root-mean-square fitting error is about 6.4 cm^{-1}. Using this PES, we present a multidimensional quantum dynamics study on tunneling splittings with an efficient theoretical scheme developed by our group. The ground-state tunneling splitting of FAD calculated with a four-mode coupled method is in good agreement with the most recent experimental measurements. The PES can be applied for further dynamics studies. The effectiveness of the present scheme for constructing a high-dimensional PES is demonstrated, and this scheme is expected to be feasible for larger molecular systems.

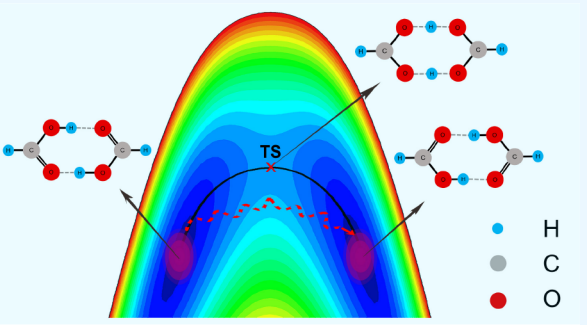

1. INTRODUCTION

Hydrogen or proton transfer plays key roles in many chemical and biological processes,[1−3] and the formic acid dimer (FAD) is an important benchmark system for studies on the double proton transfer,[2] which has attracted much research attention. Tunneling splitting is the critical observable for the study of proton-transfer dynamics,[4−11] and it can provide direct information about the isomerization rate and isomer lifetime. In the FAD case, the tunneling splittings can be produced by tunneling between symmetrically equivalent FAD wells separated by a barrier (see Figure 1), and this process is achieved via double proton transfer. Actually, FAD is regarded as the simplest concerted double-proton-transfer system,[12] whereas the simplest system for the study of sequential double proton transfer is vinylidene-acetylene.[13−16]

Experimentally, the tunneling splittings in FAD have been measured, and the values for the ground state have been obtained with increasing accuracy.[4,5,11,17−19] The Havenith group[5,18] measured the ground-state tunneling splitting of $(HCOOH)_2$ with the splitting value being reported as 0.0158 cm^{-1}. In 2014, the Duan group[11] measured the vibration−rotation−tunneling absorption spectra, and in 2017 they[19] further improved the experimental accuracy, updating the value to be 0.011367(92) cm^{-1}. Most recently, Li et al.[17] confirmed Duan's updated value by a microwave spectroscopy experiment and established 0.01117 cm^{-1} as the most accurate ground-state splitting value of FAD. In addition, a few experimental measurements of tunneling splittings upon vibrational excitation have also been reported.[5,19] Theoretically, the tunneling splittings in FAD have been calculated using various approximate methods.[20−26]

The full-dimensional *ab initio* potential energy surfaces (PES) of a reactive system is crucial for further dynamics studies. In 2016, Qu and Bowman[27] constructed the first full-dimensional *ab initio* PES (or the QB PES) for FAD based on an accurate fit of 13475 CCSD(T)-F12a/haTZ points, which was used in the study on the double-proton-transfer process in FAD. Later, Richardson[28] performed calculations using this PES and obtained interesting results about ground-state tunneling splitting. Using the QB PES, Liu et al.[29,30] studied tunneling splittings both for the ground state and upon fundamental excitation in FAD based upon a quantum dynamics (QD) scheme developed by them. An unprecedented overall agreement[31] with experimental spectra was achieved by QD calculations on the QB PES. However, Qu and Bowman also discussed[31] the quantitative differences that exist between the quantum and experimental spectra and stated that this might be due to some deficiencies in the PES. For example, the harmonic frequency of the infrared-active OH stretch differs from the benchmark frequency[32] by 20 cm^{-1}. More recently, Meuwly and co-workers[33] constructed machine-learned PESs for FAD at the

Received: March 31, 2023
Accepted: April 19, 2023
Published: May 2, 2023

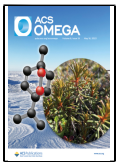

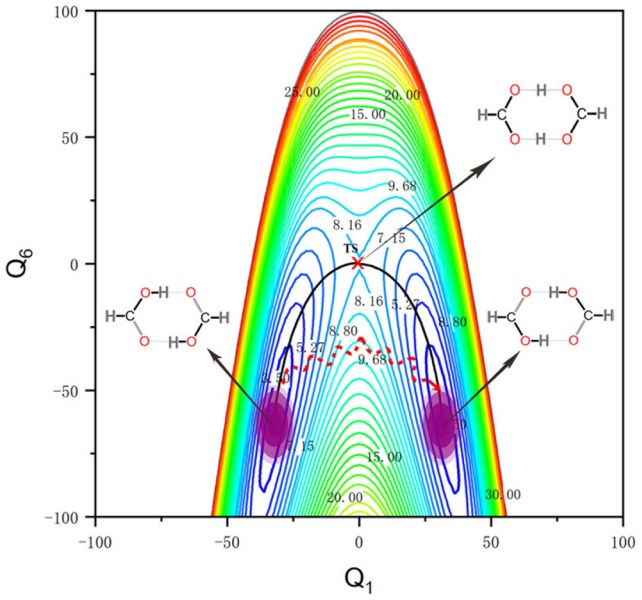

Figure 1. Contour plot of the typical regions of potential energy surface for the formic acid dimer against the relevant normal mode coordinates (Q_i, in au), with the other normal coordinates fixed at zero and energies given in kcal/mol. Schematics of the minimum energy reaction path and tunneling path for proton transfer are also indicated.

MP2 and transfer-learned to the CCSD(T) levels. The MP2 PES is represented by a neural network (NN) of the PhysNet architecture,[34] in which the parameters are fitted to *ab initio* energies. To improve the quality of this PES, they accomplished the transfer learning (TL) from the MP2 to the CCSD(T) level. The training set of TL contained 441 geometries which were calculated at the CCSD(T)/AVTZ level. Using the TL PES, the infrared spectra were calculated by finite-temperature molecular dynamics simulations and the agreement with experiment[35] was very good. Nevertheless, it seems that the TL PES underestimates the isomerization barrier height and harmonic frequencies of the OH stretch vibrations in comparison with the benchmark values.[32]

In this work we construct an accurate *ab initio* PES with a fundamental invariant NN fitting method and calculate the tunneling splittings in FAD using this PES with an efficient QD scheme developed by us. This paper is organized as follows. The details of the potential energy surface are given in section 2, and quantum tunneling dynamics methods are described in section 3. Results and discussion are presented in section 4. Finally, a summary is provided in section 5.

2. THE POTENTIAL ENERGY SURFACE

2.1. *Ab Initio* Calculations. The calculational details are as follows. The single-point energy calculations are performed by the domain-based coupled cluster theory DLPNO-CCSD(T)[36,37] with the TightPNO[38] settings, using the augmented correlation-consistent basis set aug-cc-pVnZ[39,40] (n = T). DLPNO-CCSD(T)/TightPNO/aug-cc-pVTZ is also performed for stationary-point structure optimization. The subsequent numerical harmonic frequency calculations reveal that the transition state has a single imaginary frequency. All calculations are performed with the ORCA program package based on version 4.2.0.[41]

Our geometry optimization calculations indicate that the two minima corresponding to two FAD isomers (see Figure 1) are separated by an energy barrier of 8.175 kcal/mol, or 2859 cm^{-1}. The barrier height results calculated from different levels of theory are given in Table 1 for comparison. From Table 1, we see

Table 1. Barrier Heights (cm^{-1}) for Double Proton Transfer in Formic Acid Dimer from Different Calculations[a]

method	optimization level	reference	barrier height (cm^{-1})
DLPNO-CCSD(T)/AVTZ	DLPNO-CCSD(T)/AVTZ	this work	2859
CCSD(T)-F12a/haTZ	CCSD(T)-F12a/haDZ	27	2853
CCSD(T)/AV5Z	MP2/AV5Z	42	2903
MP2/AVTZ	MP2/AVTZ	33	2340
TL-CCSD(T)/AVTZ[b]		33	2770

[a]The methods used for the single-point calculation and corresponding geometry optimization levels are indicated, respectively. [b]This level is reached by transfer learning,[33] and direct calculations are not performed.

that the barrier height obtained in this work agrees very well with that from the previous CCSD(T)-F12a/haTZ calculation.[27] Since the CCSD(T)/AV5Z single-point energy calculations[42] yield a barrier height of 2903 cm^{-1}, we suppose the true barrier height to be somewhat larger than 2860 cm^{-1}, and thus the barrier heights (2340 and 2770 cm^{-1}) obtained by Meuwly and co-workers[33] may be too low. In brief, for the purpose of PES construction, large-scale *ab initio* calculations are performed using the DLPNO-CCSD(T)/aug-cc-pVTZ method at over 14000 symmetry-unique geometries covering various PES regions. The geometries are selected from the minimum energy path, a previous geometry set,[27] normal-mode vibrational grid points, and our quasi-classical trajectory calculations.

2.2. Neural Network Fitting. The fitting is a key step in the construction of a PES.[43−46] In recent years, a series of accurate PESs for polyatomic molecules have been fitted by robust machine-learning methods such as artificial neural networks.[45,47−52] In this work, we construct the PES using a general NN fitting procedure combined with the fundamental invariant (FI) method.[45,47] The FI-NN method could be regarded as an improvement of the PIP-NN method,[48,49,53] in which the permutationally invariant polynomials (PIP) are used in the input layer of NN fitting, and both methods can incorporate the permutational symmetry with respect to identical nuclei in the fitting.

FIs transformed from internuclear distances (first to Morse-like variables and then to the FIs) are used as the input vector to guarantee the permutational symmetry of identical atoms. The Morse-like variables used in the permutationally invariant polynomial fitting approach of Bowman and co-workers[27,43] are applied, which have the form

$$M_{ij} = e^{-r_{ij}/2} \quad (1)$$

where, r_{ij} (i = 1, ..., 9; $j = i + 1$, ..., 10) are the distances between atom i and atom j, and M_{ij} are the corresponding Morse-like variables. The FI code provided by Chen et al.[45] for the $A_4B_4C_2$ system is then employed to transform the 45 Morse-like variables to 1546 polynomials with a maximum degree of 5.

The feed-forward NN employed in our fitting procedure contains two hidden layers with sigmoid-like transfer functions to provide a reasonable flexibility for surface fitting. After several tests, the structure of the NN is set to 1546-5-18-1, indicating

https://doi.org/10.1021/acsomega.3c02169
ACS Omega 2023, 8, 17296−17303

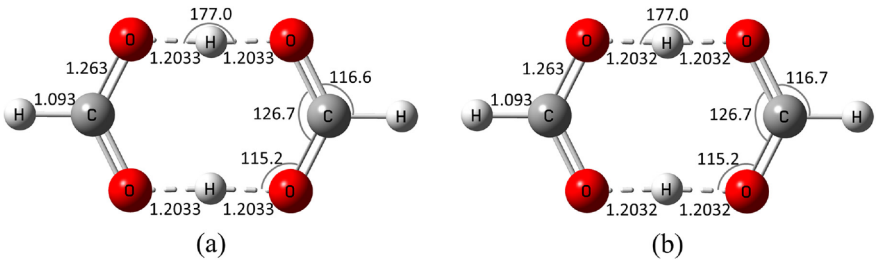

Figure 2. Key geometrical parameters of the saddle point of the formic acid dimer from the DLPNO-CCSD(T)/AVTZ calculations (a) and the present NN PES (b). Bond lengths are given in angstroms and angles in degrees.

the number of neurons in each layer. The transfer functions of the neurons in input and output layers are linear functions, and those in the hidden layers are chosen to be hyperbolic tangents. Thus, the functional form of the NN can be written as

$$E = b_{1,4} + \sum_{i=1}^{18} \left(w_{i,3} \cdot \tanh\left(b_{i,3} + \sum_{j=1}^{5} \left(w_{j,2} \cdot \tanh\left(b_{j,2} + \sum_{k=1}^{1546} (w_{k,1} \cdot \mathrm{FI}_k) \right) \right) \right) \right) \quad (2)$$

where FI_k (k = 1, ..., 1546) is the input vector, tanh is the hyperbolic tangent function, $w_{i,j}$ and $b_{i,j}$ are the weights and biases for the ith neuron of the jth layer, respectively, and E is the output energy. The weights and biases are optimized using the Levenberg−Marquardt (LM) algorithm[54] in each fitting to minimize the error. The "early stopping" method[55] is used to avoid overfitting, with 70% of the data points being randomly picked as the training set, half of the rest 30% as the validating set, and the remaining points as the testing set. The fitting procedure is stopped under such conditions:

(a) The mean-square error gradient of each epoch is smaller than 10^{-10} kcal/(mol epoch).
(b) The damping factor μ in the LM algorithm is larger than 10^{10}.
(c) The root-mean-square error (RMSE) of validating set keeps growing for 10 epochs.

Additionally, bits of improper results are screened out by examining contour plots. The quality of the fitted NN is measured by RMSE, and 6 best FI-NN fits are averaged over to further reduce the fitting error.

The energy-weighted RMSE (wRMSE) with a weight assigned to each point of the *ab initio* data is used to evaluate the fitting error of the regions we are concerned about, given by

$$\mathrm{wRMSE} = \sqrt{\frac{\sum_{i=1}^{N} (w_i \cdot (E_i^{\mathrm{PES}} - E_i^{\mathrm{ab}}))^2}{N}} \quad (3)$$

$$w_i = 0.004/(0.02 + E_i^{\mathrm{ab}})(0.2 + E_i^{\mathrm{ab}}) \quad (4)$$

where N is the total number of points we have used, E_i^{ab} is the *ab initio* energy of the point relative to the global minimum, and E_i^{PES} and w_i are the corresponding fitted energy and weight factor, respectively. In eq 4, E_i^{ab} is given in hartree.

The present NN fit totally uses over 14000 geometries and corresponding energies. The obtained NN PES has a RMSE of 0.12 kcal/mol and a maximum error of 3.25 kcal/mol for the whole data set. The RMSEs for energy points below 50 and 95 kcal/mol (the energy of the lowest point in *ab initio* calculations is taken to be zero), are 0.058 and 0.077 kcal/mol, respectively, while the corresponding maximum errors are 0.91 and 1.47 kcal/mol, respectively. The overall energy-weighted RMSE is only 0.0183 kcal/mol, or 6.4 cm^{-1}. The mean absolute error for 6397 energies that are less than 4000 cm^{-1} is about 5.0 cm^{-1}. These indicate that the current fitting reaches a high accuracy.

3. QUANTUM DYNAMICS METHOD

The Bian group has developed an efficient theoretical scheme in which the process-oriented basis function customization (PBFC) strategy[3,56] is combined with the preconditioned inexact spectral transform (PIST) method.[57−61] The basis idea of PBFC is to customize basis functions for a specific chemical process by optimizing and adjusting the n-dimensional (nD) effective potential (EP), and it is very effective in reducing the overall basis size and raising the computational efficiency. Generally speaking, the obtained nD EPs and coordinate ranges are oriented toward the double-proton-transfer process. In particular, the optimized ranges for the coordinates of in-plane vibrational modes are much larger than those for the coordinates of out-of-plane modes, since the double-proton-transfer process mainly occurs within the plane.

In the present QD treatment, we choose the saddle point as the reference point of normal coordinates for the Hamiltonian, and the M-mode effective normal Hamiltonian for J = 0 is written as[29,60]

$$\hat{H} = -\frac{1}{2} \sum_{i=1}^{M} \frac{\partial^2}{\partial Q_{k_i}^2} + V(Q_{k_1}, Q_{k_2}, ..., Q_{k_M}) \quad (5)$$

where V is the EP, Q_{k_i} denotes one of the mass-rescaled normal coordinates obtained at the saddle point, and M = 1, 2, 3, ... here. The vibrational angular momenta (VAM) are neglected, which is justified by the fact that the VAM terms are very small and basically constant along the reaction path. Thus, the contribution of VAM terms to the ground-state tunneling splitting is negligible. Here the MD EP $V(Q_{k_1}, Q_{k_2}, \cdots, Q_{k_M})$ is generated based upon the PBFC strategy, and the modes which are essential to the concerned specific proton-transfer process should be incorporated into calculations. The normal-mode analysis is performed on the present PES, and Q_1 is the main proton-transfer reaction coordinate.

The total wave function is expanded by the direct product of 1D discrete variable representation (DVR) basis functions

$$\Psi = \sum_{i_{k_1}=1}^{N_{k_1}} \cdots \sum_{i_{k_M}=1}^{N_{k_M}} c_{i_{k_1} \cdots i_{k_M}} \prod_{j=1}^{M} \pi_{i_{k_j}}(Q_{k_j}) \quad (6)$$

https://doi.org/10.1021/acsomega.3c02169
ACS Omega 2023, 8, 17296−17303

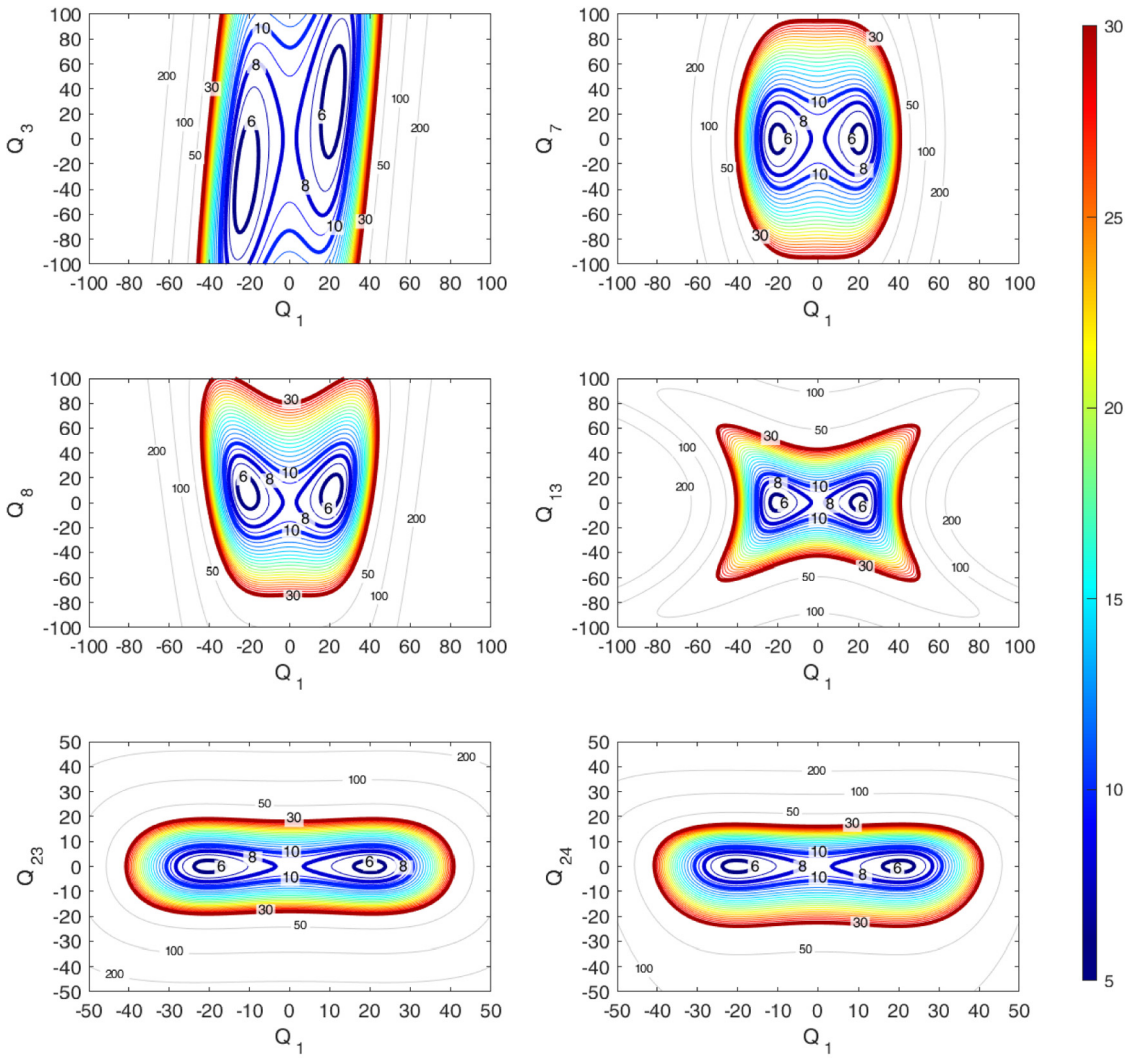

Figure 3. Contour plots of the selected PES regions against the relevant saddle-point normal mode coordinates (Q_i), with the other normal coordinates fixed at zero (Q_i in au and energies in kcal/mol).

where $\pi_{i_{k_j}}(Q_{k_j})$ is the 1D DVR basis function for Q_{k_j} with a basis size of N_{k_j}. The 1D DVR basis functions are generated from 1D EPs acquired according to the PBFC strategy.[29,62] The implementation of the PIST method has been extended to molecular systems with 4 and more atoms by us, and some details are given below. In terms of the basis expansion, we separate the basis functions into the inner and outer groups, which is helpful to acquire a sparse and well-structured matrix. For example, in the 4D case we arrange (Q_3, Q_6, and Q_8) as the outer group, whereas (Q_1) is treated as the inner group. Then the PIST method combined with an optimal separable basis plus Wyatt (OSBW) preconditioner is used to solve the resultant eigenvalue problem.[59,63−65] Furthermore, the time-consuming parts of our scheme are parallelized.

4. RESULTS AND DISCUSSION

4.1. Properties of the PES. The global *ab initio* NN PES newly constructed in this work reproduces the *ab initio* data very well. The barrier height of the present NN PES is 2860 cm^{-1}, in excellent agreement with the value of 2859 cm^{-1} calculated with the DLPNO-CCSD(T)/AVTZ method (see Table 1). The configurations and key geometrical parameters of the saddle point from the present NN PES and DLPNO-CCSD(T)/AVTZ calculations are shown in Figure 2. We see that the results from the PES agree well with those from the direct DLPNO-CCSD(T)/AVTZ calculations.

To make sure that our surface can describe all dynamically important regions properly, we make contour plots in various regions and check the structures carefully. This is achieved by transforming to FAD normal coordinates at the saddle point (see Table S1 of the Supporting Information (SI) for the physical description) and then plotting it against specific normal coordinates with the other coordinates fixed. Typical contour plots for several important regions are shown in Figure 3 to demonstrate the accurate behavior of the present full-dimensional PES. Generally speaking, all of the figures are smooth and are physically reasonable.

Additionally, the harmonic frequencies of the formic acid dimer at the minimum geometries are calculated from the present NN PES and are given in Table 2, along with results from the literature. We see from Table 2 that our results are in very good general agreement with the *ab initio* calculational results at the CCSD(T)/AVQZ level, which are the most accurate available values.[32] The RMS error for frequencies of all 24 modes on our PES is only 4.6 cm^{-1}. Although the QB PES is

https://doi.org/10.1021/acsomega.3c02169
ACS Omega 2023, 8, 17296−17303

Table 2. Harmonic Frequencies (cm^{-1}) of the Formic Acid Dimer at the Minimum Geometries, from Different PESs in Comparison with the CCSD(T)/AVQZ Benchmark

mode	present PES	QB PES[a]	TL PES[b]	CCSD(T)-F12a/haDZ[c]	CCSD(T)/AVQZ[d]
1	71	70	70	92	72
2	169	167	168	183	167
3	175	170	176	222	177
4	210	209	211	230	209
5	253	254	253	290	255
6	276	275	277	293	275
7	687	693	682	691	684
8	716	716	711	716	712
9	961	956	964	972	963
10	981	970	987	989	986
11	1082	1084	1080	1093	1079
12	1103	1100	1102	1094	1099
13	1255	1255	1250	1260	1252
14	1260	1258	1255	1263	1256
15	1404	1406	1402	1396	1405
16	1411	1408	1404	1422	1409
17	1462	1448	1458	1466	1455
18	1490	1481	1487	1492	1481
19	1715	1715	1708	1721	1713
20	1778	1780	1772	1785	1777
21	3092	3095	3094	3101	3099
22	3092	3097	3098	3107	3103
23	3210	3232	3189	3204	3204
24	3313	3326	3293	3303	3306

[a]From the PES of Qu and Bowman.[27] [b]From the transfer-learned PES.[33] [c]From the CCSD(T)-F12a/haDZ calculations of ref 27. [d]From the CCSD(T)/AVQZ calculations of ref 32.

of very high quality, Qu and Bowman discussed[31] some deficiencies in the QB PES, which can explain the quantitative differences between the quantum and experimental spectra. In particular, they[31] mentioned that the harmonic frequency of the infrared-active (or antisymmetric) OH stretch on the QB PES differs from the benchmark frequency[32] by 20 cm^{-1}. The minimum-point normal mode coordinates Q_{23} and Q_{24} indicate the OH symmetric and antisymmetric stretch modes, respectively, and pictures and descriptions of these normal modes are given in Figure 4. From Table 2, we see that the harmonic frequencies of the OH antisymmetric stretch (Q_{24}) are 3313 cm^{-1} on our PES and 3293 cm^{-1} on the TL PES, respectively, which indicates that the TL PES underestimates the frequency by 13 cm^{-1}, and our PES is in better agreement with the benchmark value. In addition, for the harmonic frequency of the OH symmetric stretch (Q_{23}), the QB PES overestimates it by 28 cm^{-1}, whereas the TL PES underestimates it by 15 cm^{-1}, compared with the benchmark value[32] of 3204 cm^{-1}, which is in very good agreement with the value obtained on the present PES. So, for the harmonic frequencies for the OH symmetric and antisymmetric stretches (or Q_{23} and Q_{24}), better agreement with benchmark values is achieved on our PES; those frequencies are underestimated on the TL PES and overestimated on the QB PES to some extent. These kinds of deviations should come from the *ab initio* QB and TL PESs used in the vibrational calculations, indicating that the PES region associated with the OH stretch modes (see Figure 4) may need to be modified.

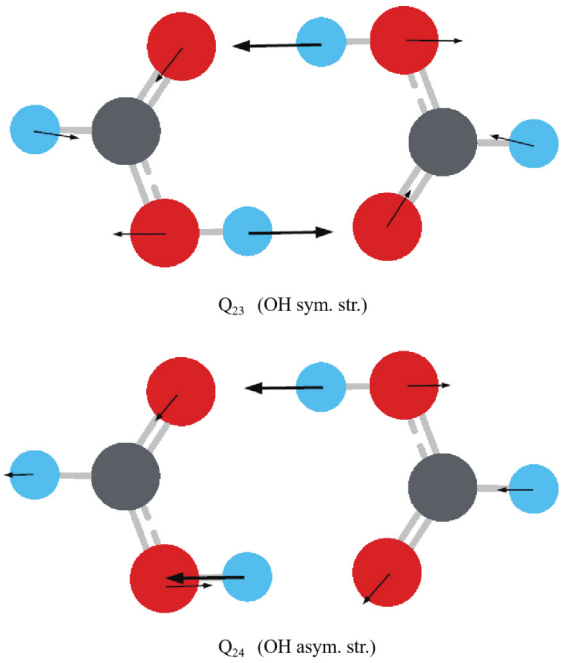

Figure 4. Vibrational modes of the formic acid dimer. The upper panel shows the OH symmetric stretch motion, whereas the lower panel shows the OH antisymmetric stretch. The minimum-point normal mode coordinates are also indicated.

4.2. Ground-State Tunneling Splitting. Various multidimensional QD calculations are performed with the above scheme on the global *ab initio* NN PES constructed in this work. The tunneling splittings can be produced by tunneling through the barrier between the two isomers (see Figure 1). Previous work[27] has shown that, besides the Q_1 mode, the Q_6, Q_3, and Q_8 modes are important in the process of proton transfer and need to be considered in the multidimensional QD calculations. In each calculation, the Lanczos iteration tolerance is set as 10^{-6} cm^{-1} and the iteration deviation for the obtained eigenenergy is less than 10^{-7} cm^{-1}. The number of iterations is about 1400 in the QMR procedure and about 100 in the Lanczos procedure. Our test 1−4D calculations indicate that, with the basis size ($N_{Q_1} = 32$, $N_{Q_6} = 13$, $N_{Q_3} = 13$, $N_{Q_8} = 11$), we can obtain converged energy levels required for the study of ground-state tunneling splittings. The tunneling splittings calculated with different multidimensional models are presented in Table 3. From Table 3, we can notice an interesting decreasing trend from left to right, for both our calculational and experimental results. This trend actually corresponds to an increasing accuracy. Microwave spectroscopy,[17] yielding a splitting value of 0.01117 cm^{-1}, is of much higher resolution than the spectroscopy measurements reported much earlier.[5] As shown, our 4D results agree well with the most recent experimental measurements using microwave spectroscopy.

It can also be seen from Table 3 that the obtained tunneling splittings are generally small, indicating a long lifetime of the FAD isomer, which can be explained by the relatively weak deep tunneling through the barrier. The largest tunneling splitting is obtained in the 1D case, which has a value of 0.462 cm^{-1}, in excellent agreement with the calculated values reported by Qu and Bowman[27] (0.44 cm^{-1}) and Richardson[28] (0.47 cm^{-1}). This is a good verification of different QD methods and also indicates that the 1D minimum energy reaction path of the present NN

https://doi.org/10.1021/acsomega.3c02169
ACS Omega 2023, 8, 17296−17303

Table 3. Calculated Ground-State Tunneling Splittings (in cm^{-1}) for the Formic Acid Dimer, in Comparison with the Experimental Measurements

this work[a]					experiment		
1D	2D[1]	2D[2]	3D	4D	2007[b]	2017[c]	2019[d]
0.462	0.0687	0.0383	0.0154	0.0128	0.0158	0.011367	0.01117

[a]Calculations are performed with the 1D (Q_1), 2D[1] (Q_1, Q_6), 2D[2] (Q_1, Q_3), 3D (Q_1, Q_6, Q_3) and 4D (Q_1, Q_6, Q_3, Q_8) models, respectively. [b]The experimental value measured in ref 5. [c]The value is obtained in ref 19 by measuring the vibration−rotation−tunneling absorption spectra. [d]The value is reported in ref 17 by a microwave spectroscopy experiment.

PES is similar to that of the QB PES. It is understandable that the tunneling splitting goes down from 1D to 4D models, indicating a gradually slowing down tunneling rate, since it is known that the Q_6, Q_3, and Q_8 modes[27] have strong couplings with the Q_1 mode, which is the main isomerization coordinate in the double-proton-transfer process, and these kinds of couplings can hinder the proton transfer. However, the difference between the results of the 3D and 4D models is not large, and the couplings of other FAD modes with the Q_1 mode are much smaller, and thus we estimate that the splitting for the ground state would not change evidently if we include more modes into the models.

5. CONCLUSIONS

Summing up, we construct a new full-dimensional *ab initio* NN PES for the formic acid dimer. The DLPNO-CCSD(T)/aug-cc-pVTZ calculations have been performed at over 14000 symmetry-unique geometries, and an accurate fit to the obtained energy points is achieved using a general NN fitting procedure combined with the FI method. The overall energy-weighted RMS fitting error is only about 6.4 cm^{-1}, and the accuracy of this PES is further demonstrated by vibrational and tunneling splitting calculations. Using this PES, we have performed reduced-dimensionality quantum tunneling dynamics calculations using an efficient PBFC-PIST theoretical scheme developed in our group, and the obtained ground-state tunneling splitting of FAD is in good agreement with the most recent experimental measurements.

In this work the application of the FI method is extended to a 10-atom molecular system with complete consideration of the permutational symmetry of identical atoms. The present scheme for constructing a high-dimensional PES is efficient, which is feasible for larger molecular systems and provides us a good starting point for treating more complicated systems such as the FAD-furan complex. In addition, further theoretical calculations using our PES are required. The present PES can be used for further dynamics studies of the double-proton-transfer processes in FAD, and further calculations of various vibrational states and spectra of FAD.

The codes for the present potential energy surface are available from the corresponding author upon request and at http://159.226.64.162/web/49818/downloads.

■ ASSOCIATED CONTENT

Data Availability Statement

All the data that support the findings of this study are available within the article/Supporting Information and from the corresponding author upon reasonable request.

Supporting Information

The Supporting Information is available free of charge at https://pubs.acs.org/doi/10.1021/acsomega.3c02169.

FAD normal coordinates, physical descriptions, and the normal frequencies on the present LYLCB (Li−Yang−Liu−Cao−Bian) PES; parameters for the present PES (PDF)

■ AUTHOR INFORMATION

Corresponding Author

Wensheng Bian − *Beijing National Laboratory for Molecular Sciences, Institute of Chemistry, Chinese Academy of Sciences, Beijing 100190, People's Republic of China; School of Chemical Sciences, University of Chinese Academy of Sciences, Beijing 100049, People's Republic of China;* orcid.org/0000-0003-2125-8054; Email: bian@iccas.ac.cn

Authors

Fengyi Li − *Beijing National Laboratory for Molecular Sciences, Institute of Chemistry, Chinese Academy of Sciences, Beijing 100190, People's Republic of China; School of Chemical Sciences, University of Chinese Academy of Sciences, Beijing 100049, People's Republic of China*

Xingyu Yang − *Beijing National Laboratory for Molecular Sciences, Institute of Chemistry, Chinese Academy of Sciences, Beijing 100190, People's Republic of China; School of Chemical Sciences, University of Chinese Academy of Sciences, Beijing 100049, People's Republic of China*

Xiaoxi Liu − *Beijing National Laboratory for Molecular Sciences, Institute of Chemistry, Chinese Academy of Sciences, Beijing 100190, People's Republic of China; School of Chemical Sciences, University of Chinese Academy of Sciences, Beijing 100049, People's Republic of China*

Jianwei Cao − *Beijing National Laboratory for Molecular Sciences, Institute of Chemistry, Chinese Academy of Sciences, Beijing 100190, People's Republic of China;* orcid.org/0000-0003-0887-1110

Complete contact information is available at: https://pubs.acs.org/10.1021/acsomega.3c02169

Author Contributions

F.L. and X.Y. contributed equally to this work.

Notes

The authors declare no competing financial interest.

■ ACKNOWLEDGMENTS

This work was supported by the National Natural Science Foundation of China (Nos. 22133003, 21973098) and the Beijing National Laboratory for Molecular Sciences. J.C. acknowledges the Youth Innovation Promotion Association CAS (No. 2018045).

■ REFERENCES

(1) Vdovin, A.; Sepioł, J.; Urbańska, N.; Pietraszkiewicz, M.; Mordziński, A.; Waluk, J. Evidence for Two Forms, Double Hydrogen Tunneling, and Proximity of Excited States in Bridge-Substituted

Porphycenes: Supersonic Jet Studies. *J. Am. Chem. Soc.* **2006**, *128*, 2577−2586.
(2) Smedarchina, Z.; Siebrand, W.; Fernández-Ramos, A. Zero-Point Tunneling Splittings in Compounds with Multiple Hydrogen Bonds Calculated by the Rainbow Instanton Method. *J. Phys. Chem. A* **2013**, *117*, 11086−11100.
(3) Wu, F.; Ren, Y.; Bian, W. The Hydrogen Tunneling Splitting in Malonaldehyde: A Full-Dimensional Time-Independent Quantum Mechanical Method. *J. Chem. Phys.* **2016**, *145*, 074309.
(4) Madeja, F.; Havenith, M. High Resolution Spectroscopy of Carboxylic Acid in the Gas Phase: Observation of Proton Transfer in $(DCOOH)_2$. *J. Chem. Phys.* **2002**, *117*, 7162−7168.
(5) Ortlieb, M.; Havenith, M. Proton Transfer in $(HCOOH)_2$: An IR High-Resolution Spectroscopic Study of the Antisymmetric C-O Stretch. *J. Phys. Chem. A* **2007**, *111*, 7355−7363.
(6) Yu, H.-G.; Song, H.; Yang, M. A Rigorous Full-Dimensional Quantum Dynamics Study of Tunneling Splitting of Rovibrational States of Vinyl Radical C_2H_3. *J. Chem. Phys.* **2017**, *146*, 224307.
(7) Braams, B. J.; Yu, H. G. Potential Energy Surface and Quantum Dynamics Study of Rovibrational States for HO_3 (X^2A''). *Phys. Chem. Chem. Phys.* **2008**, *10*, 3150−3155.
(8) Arabi, A. A.; Matta, C. F. Effects of External Electric Fields on Double Proton Transfer Kinetics in the Formic Acid Dimer. *Phys. Chem. Chem. Phys.* **2011**, *13*, 13738−13748.
(9) Luckhaus, D. Concerted Hydrogen Exchange Tunneling in Formic Acid Dimer. *J. Phys. Chem. A* **2006**, *110*, 3151−3158.
(10) Jain, A.; Sibert, E. L. Tunneling Splittings in Formic Acid Dimer: An Adiabatic Approximation to the Herring Formula. *J. Chem. Phys.* **2015**, *142*, 084115.
(11) Goroya, K. G.; Zhu, Y.; Sun, P.; Duan, C. High Resolution Jet-Cooled Infrared Absorption Spectra of the Formic Acid Dimer: A Reinvestigation of the C-O Stretch Region. *J. Chem. Phys.* **2014**, *140*, 164311.
(12) Kim, Y. Direct Dynamics Calculation for the Double Proton Transfer in Formic Acid Dimer. *J. Am. Chem. Soc.* **1996**, *118*, 1522−1528.
(13) DeVine, J. A.; Weichman, M. L.; Laws, B.; Chang, J.; Babin, M. C.; Balerdi, G.; Xie, C.; Malbon, C. L.; Lineberger, W. C.; Yarkony, D. R.; et al. Encoding of Vinylidene Isomerization in Its Anion Photoelectron Spectrum. *Science* **2017**, *358*, 336−339.
(14) DeVine, J. A.; Weichman, M. L.; Xie, C.; Babin, M. C.; Johnson, M. A.; Ma, J.; Guo, H.; Neumark, D. M. Autodetachment from Vibrationally Excited Vinylidene Anions. *J. Phys. Chem. Lett.* **2018**, *9*, 1058−1063.
(15) Luo, J.; Cao, J.; Liu, H.; Bian, W. Accurate Quantum Mechanical Calculations on Deuterated Vinylidene Isomerization. *J. Chem. Phys.* **2020**, *153*, 054309.
(16) Luo, J.; Cao, J.; Liu, H.; Bian, W. Accurate Quantum Dynamics of the Simplest Isomerization System Involving Double-H Transfer. *Chin. J. Chem. Phys.* **2022**, *35*, 185−192.
(17) Li, W.; Evangelisti, L.; Gou, Q.; Caminati, W.; Meyer, R. The Barrier to Proton Transfer in the Dimer of Formic Acid: A Pure Rotational Study. *Angew. Chem., Int. Ed.* **2019**, *58*, 859−865.
(18) Gutberlet, A.; Schwaab, G. W.; Havenith, M. High Resolution IR Spectroscopy of the Carbonyl Stretch of $(DCOOD)_2$. *Chem. Phys.* **2008**, *343*, 158−167.
(19) Zhang, Y.; Li, W.; Luo, W.; Zhu, Y.; Duan, C. High Resolution Jet-Cooled Infrared Absorption Spectra of $(HCOOH)_2$, $(HCOOD)_2$, and HCOOH-HCOOD Complexes in 7.2 μm Region. *J. Chem. Phys.* **2017**, *146*, 244306.
(20) Chang, Y. T.; Yamaguchi, Y.; Miller, W. H.; Schaefer, H. F. An Analysis of the Infrared and Raman Spectra of the Formic Acid Dimer $(HCOOH)_2$. *J. Am. Chem. Soc.* **1987**, *109*, 7245−7253.
(21) Ushiyama, H.; Takatsuka, K. Successive Mechanism of Double-Proton Transfer in Formic Acid Dimer: A Classical Study. *J. Chem. Phys.* **2001**, *115*, 5903−5912.
(22) Smedarchina, Z.; Fernández-Ramos, A.; Siebrand, W. Tunneling Dynamics of Double Proton Transfer in Formic Acid and Benzoic Acid Dimers. *J. Chem. Phys.* **2005**, *122*, 134309.
(23) Mil'nikov, G. V.; Kühn, O.; Nakamura, H. Ground-State and Vibrationally Assisted Tunneling in the Formic Acid Dimer. *J. Chem. Phys.* **2005**, *123*, 074308.
(24) Barnes, G. L.; Squires, S. M.; Sibert, E. L. Symmetric Double Proton Tunneling in Formic Acid Dimer: A Diabatic Basis Approach. *J. Phys. Chem. B* **2008**, *112*, 595−603.
(25) Barnes, G. L.; Sibert, E. L. The Effects of Asymmetric Motions on the Tunneling Splittings in Formic Acid Dimer. *J. Chem. Phys.* **2008**, *129*, 164317.
(26) Luckhaus, D. Hydrogen Exchange in Formic Acid Dimer: Tunnelling Above the Barrier. *Phys. Chem. Chem. Phys.* **2010**, *12*, 8357−8361.
(27) Qu, C.; Bowman, J. M. An ab initio Potential Energy Surface for the Formic Acid Dimer: Zero-Point Energy, Selected Anharmonic Fundamental Energies, and Ground-State Tunneling Splitting Calculated in Relaxed 1−4-mode Subspaces. *Phys. Chem. Chem. Phys.* **2016**, *18*, 24835−24840.
(28) Richardson, J. O. Full- and Reduced-Dimensionality Instanton Calculations of the Tunnelling Splitting in the Formic Acid Dimer. *Phys. Chem. Chem. Phys.* **2017**, *19*, 966−970.
(29) Liu, H.; Cao, J.; Bian, W. Double Proton Transfer in the Dimer of Formic Acid: An Efficient Quantum Mechanical Scheme. *Front. Chem.* **2019**, *7*, 676.
(30) Liu, H.; Cao, J.; Bian, W. Efficient Quantum Mechanical Calculations of Mode-Specific Tunneling Splittings upon Fundamental Excitation in the Dimer of Formic Acid. *J. Phys. Chem. A* **2020**, *124*, 6536−6543.
(31) Qu, C.; Bowman, J. M. Quantum and Classical IR spectra of $(HCOOH)_2$,$(DCOOH)_2$ and $(DCOOD)_2$ using ab initio potential energy and dipole moment surfaces. *Faraday Discuss.* **2018**, *212*, 33−49.
(32) Miliordos, E.; Xantheas, S. S. On the Validity of the Basis Set Superposition Error and Complete Basis Set Limit Extrapolations for the Binding Energy of the Formic Acid Dimer. *J. Chem. Phys.* **2015**, *142*, 094311.
(33) Käser, S.; Meuwly, M. Transfer Learned Potential Energy Surfaces: Accurate Anharmonic Vibrational Dynamics and Dissociation Energies for the Formic Acid Monomer and Dimer. *Phys. Chem. Chem. Phys.* **2022**, *24*, 5269−5281.
(34) Unke, O. T.; Meuwly, M. PhysNet: A Neural Network for Predicting Energies, Forces, Dipole moments, and Partial Charges. *J. Chem. Theory Comput.* **2019**, *15*, 3678−3693.
(35) Nejad, A.; Meyer, K. A. E.; Kollipost, F.; Xue, Z.; Suhm, M. A. Slow Monomer Vibrations in Formic Acid Dimer: Stepping up the Ladder with FTIR and Raman Jet Spectroscopy. *J. Chem. Phys.* **2021**, *155*, 224301.
(36) Riplinger, C.; Sandhoefer, B.; Hansen, A.; Neese, F. Naturaltriple Excitations in Local Coupled Cluster Calculations with Pair Natural Orbitals. *J. Chem. Phys.* **2013**, *139*, 134101.
(37) Riplinger, C.; Pinski, P.; Becker, U.; Valeev, E. F.; Neese, F. Sparse Maps−A Systematic Infrastructure for Reduced-Scaling Electronic Structure Methods. II. Linear Scaling Domain based Pair Natural Orbital Coupled Cluster Theory. *J. Chem. Phys.* **2016**, *144*, 024109.
(38) Liakos, D. G.; Sparta, M.; Kesharwani, M. K.; Martin, J. M. L.; Neese, F. Exploring the Accuracy Limits of Local Pair Natural Orbital Coupled-Cluster Theory. *J. Chem. Theory Comput.* **2015**, *11*, 1525−1539.
(39) van Mourik, T.; Dunning, T. H.; Peterson, K. A. Ab Initio Characterization of the HCO^x (x = −1, 0, + 1) Species: Structures, Vibrational Frequencies, CH Bond Dissociation Energies, and HCO Ionization Potential and Electron Affinity. *J. Phys. Chem. A* **2000**, *104*, 2287−2293.
(40) Dunning, T. H.; Peterson, K. A. Approximating the Basis Set Dependence of Coupled Cluster Calculations: Evaluation of Perturbation Theory Approximations for Stable Molecules. *J. Chem. Phys.* **2000**, *113*, 7799−7808.
(41) Neese, F. Software update: the ORCA program system, version 4.0. *WIREs Comput. Mol. Sci.* **2018**, *8*, No. e1327.

https://doi.org/10.1021/acsomega.3c02169
ACS Omega 2023, 8, 17296−17303

(42) Ivanov, S. D.; Grant, I. M.; Marx, D. Quantum Free Energy Landscapes from ab Initio Path Integral Metadynamics: Double Proton Transfer in the Formic Acid Dimer is Concerted but not Correlated. *J. Chem. Phys.* **2015**, *143*, 124304.
(43) Braams, B. J.; Bowman, J. M. Permutationally Invariant Potential Energy Surfaces in High Dimensionality. *Int. Rev. Phys. Chem.* **2009**, *28*, 577−606.
(44) Rocha, C. M. R.; Varandas, A. J. C. Accurate CHIPR Potential Energy Surface for the Lowest Triplet State of C_3. *J. Phys. Chem. A* **2019**, *123*, 8154−8169.
(45) Chen, R.; Shao, K.; Fu, B.; Zhang, D. H. Fitting Potential Energy Surfaces with Fundamental Invariant Neural Network. II. Generating Fundamental Invariants for Molecular Systems with up to Ten Atoms. *J. Chem. Phys.* **2020**, *152*, 204307.
(46) Song, Y. Z.; Varandas, A. J. C. Accurate Double Many-Body Expansion Potential Energy Surface for Ground-State HS_2 Based on ab Initio Data Extrapolated to the Complete Basis Set Limit. *J. Phys. Chem. A* **2011**, *115*, 5274−5283.
(47) Blank, T. B.; Brown, S. D.; Calhoun, A. W.; Doren, D. J. Neural Network Models of Potential Energy Surfaces. *J. Chem. Phys.* **1995**, *103*, 4129−4137.
(48) Jiang, B.; Guo, H. Permutation invariant polynomial neural network approach to fitting potential energy surfaces. *J. Chem. Phys.* **2013**, *139*, 054112.
(49) Li, J.; Jiang, B.; Guo, H. Permutation invariant polynomial neural network approach to fitting potential energy surfaces. II. Four-atom systems. *J. Chem. Phys.* **2013**, *139*, 204103.
(50) Cao, J.; Wu, Y.; Ma, H.; Shen, Z.; Bian, W. Dynamics and Kinetics of the Si(^{1}D) + H_2/D_2 Reactions on a New Global ab initio Potential Energy Surface. *Phys. Chem. Chem. Phys.* **2021**, *23*, 6141−6153.
(51) Lu, X.; Shang, C.; Li, L.; Chen, R.; Fu, B.; Xu, X.; Zhang, D. H. Unexpected Steric Hindrance Failure in the Gas Phase $F^-+(CH_3)_3CI$ S_N2 Reaction. *Nat. Commun.* **2022**, *13*, 4427.
(52) Cao, J.; Li, F.; Xia, W.; Bian, W. van der Waals Interactions in Bimolecular Reactions. *Chin. J. Chem. Phys.* **2019**, *32*, 157−166.
(53) Jiang, B.; Li, J.; Guo, H. Potential Energy Surfaces from High Fidelity Fitting of ab Initio Points: the Permutation Invariant Polynomial - Neural Network Approach. *Int. Rev. Phys. Chem.* **2016**, *35*, 479−506.
(54) Hagan, M.; Menhaj, M. Training Feedforward Networks with the Marquardt algorithm. *IEEE Trans. Neural Networks* **1994**, *5*, 989−993.
(55) Raff, L.; Komanduri, R.; Hagan, M.; Bukkapatnam, S. *Neural Networks in Chemical Reaction Dynamics*; Oxford University Press: 2012.
(56) Ren, Y.; Bian, W. Mode-Specific Tunneling Splittings for a Sequential Double-Hydrogen Transfer Case: An Accurate Quantum Mechanical Scheme. *J. Phys. Chem. Lett.* **2015**, *6*, 1824−1829.
(57) Huang, S.-W.; Carrington, T. A New Iterative Method for Calculating Energy Levels and Wave Functions. *J. Chem. Phys.* **2000**, *112*, 8765−8771.
(58) Poirier, B.; Carrington, T. Accelerating the Calculation of Energy Levels and Wave Functions Using an Efficient Preconditioner with the Inexact Spectral Transform Method. *J. Chem. Phys.* **2001**, *114*, 9254−9264.
(59) Poirier, B.; Carrington, T. A Preconditioned Inexact Spectral Transform Method for Calculating Resonance Energies and Widths, as Applied to HCO. *J. Chem. Phys.* **2002**, *116*, 1215−1227.
(60) Ren, Y.; Li, B.; Bian, W. Full-Dimensional Quantum Dynamics Study of Vinylidene−Acetylene Isomerization: A Scheme Using the Normal Mode Hamiltonian. *Phys. Chem. Chem. Phys.* **2011**, *13*, 2052−2061.
(61) Li, B.; Bian, W. Efficient Quantum Calculations of Vibrational States of Vinylidene in Full Dimensionality: A Scheme with Combination of Methods. *J. Chem. Phys.* **2008**, *129*, 024111.
(62) Bian, W.; Cao, J. The PBFC-PI Quantum Dynamical Method and Its Applications. *Chem. J. Chinese Universities* **2021**, *42*, 2123−2135.
(63) Wyatt, R. E. Matrix Spectroscopy: Computation of Interior Eigenstates of Large Matrices Using Layered Iteration. *Phys. Rev. E* **1995**, *51*, 3643−3658.
(64) Li, B.; Ren, Y.; Bian, W. Accurate Quantum Dynamics Study on the Resonance Decay of Vinylidene. *ChemPhysChem* **2011**, *12*, 2419−2422.
(65) Zhang, Z.; Li, B.; Shen, Z.; Ren, Y.; Bian, W. Efficient Quantum Calculation of the Vibrational States of Acetylene. *Chem. Phys.* **2012**, *400*, 1−7.

https://doi.org/10.1021/acsomega.3c02169
ACS Omega 2023, 8, 17296−17303